ORIGINAL ARTICLE

Utilizing the analytical signal method in prospecting gravity anomaly profiles

Khalid S. Essa[2] · Eid R. Abo-Ezz[1,2] · Yves Géraud[3]

Abstract

Herein, the gravity anomalies are a function of horizontal variations in subsurface rock densities; therefore, the interpretation of gravity anomalies is useful in prospecting the provinces that have contrasting geological structures, which contain crypts, minerals, ores, and hydrocarbon deposit. Depth-size relationships due to geological considerations in the region are also necessary. This study attempted to develop a new fast inversion algorithm to prospect the gravity anomaly profiles, like evaluating the depth, the amplitude coefficient, and the shape parameter of target structures for simple geometric bodies. This new inverted model parameters approach mainly used the analytical signal of the gravity anomaly profile data. The efficiency and stability of this method were tested by many cases such as noise-free and noisy synthetic cases, multiple model cases effect, and the effect of choosing the location of the origin. In addition, the validity of this method was examined by raw gravity data from three different locations around the world, Slovakia, Cuba, and India. In all the three examined real gravity data, it was reported that the estimated parameters were consistent in an appositive manner with the actual ones and with those reported by the extent of research. The necessary time to discover this proper elucidation was very short and the assessed parameters demonstrated that the new suggested method was applicable for gravity exploration. The study concludes that this method can be extracted parameters, which have a significant association in terms of geologic and economic characteristics.

Introduction

Gravity data interpretation is valuable and it is utilized in exploring archaeology, minerals, ores, and oils in different places around the world (Cella et al. 2008; Essa 2013; Mehanee 2014; Abdelrahman and Essa 2013, 2015; Mehanee and Essa 2015; Essa and Géraud 2020). Simple geometric models such as Spheres, cylinders, thin sheets or faults are considered simple geological structures because they play an important role in many exploration issues. Several interpreted approaches are often used to calculate their parameters. Furthermore, these models are not geologically exact, but they can be frequently used in gravity interpretation in evaluating the body parameters (Hinze et al. 2013; Essa et al. 2021).

The different geometrical shapes of subsurface structures confirm the inapplicability of interpreting the gravity data. This, consequently, will cause the production of a similar gravity anomaly that clearly appears on the earth's surface. Therefore, it is important to minimize these issues by increasing the completeness of the data, decreasing the measurement error of the data space, setting the appropriate parameters, and having a priori information followed by the inversion process (Abdelrahman et al. 2003; Biswas et al. 2017; Eshaghzadeh et al. 2019; Essa and Munschy 2019).

Various idealized bodies cannot be found in real subsurface geological situations. Besides, these suggested models are favored and applied in the gravity interpretation. The objective of the inversion process is to conquer the parameters of the target, i.e., shape factor, depth, and amplitude

✉ Khalid S. Essa
  khalid_sa_essa@yahoo.com

✉ Eid R. Abo-Ezz
  e.aboezz@psau.edu.sa

[1] Department of Physics, College of Science and Humanities, Prince Sattam Bin Abdulaziz University, 11942, Al-Kharj, Saudi Arabia

[2] Geophysics Department, Faculty of Science, Cairo University, Giza P.O. 12613, Egypt

[3] GeoRessources Laboratory UMR 7359, Université de Lorraine, 54000 Nancy, France

coefficient. The prior research showed and deliberated different graphical and arithmetical methods for inferring gravity data due to simple sources (Odegard and Berg 1965, Nettleton 1976, Thompson 1982, Kilty 1983, Marson and Klingele 1993, Abdelrahman et al. 2002, Abdelrahman et al. 2006, Essa 2007a, Asfahani and Tlas 2008, Abedi et al. 2009, Essa 2011). Nevertheless, the shortcomings of these methods that depend on characteristic points and curves emphasized human imprecisions in evaluating the buried structures' parameters (Essa 2014). Thus, this confirms the neediness for an accurate inversion method that produces approximately actual geometry parameters for the buried target structures.

To facilitate this study, an inversion technique based on a fast inversion method was developed using the analytical signal of gravity anomaly to appraise the parameters of the subsurface structures, namely; depth, amplitude, and shape. The analytical signal calculation depends on the derivatives which suppressed and treated different background gravity anomaly trends especially for many anomalies in lateral directions. In consistent with this, Srivastava and Agarwal (2010) and Ekinci et al. (2017) demonstrated the application of metaheuristic algorithms such as particle swarm and differential evolution to invert the magnetic anomalies through the analytical signal approach.

The objective of this study was to improve the efficient algorithm based on the simple bodies by finding a robust and exact method for simple model structures elucidation and examining the uncertainty in explanation and conceivable method to avoid vagueness for a consistent result. In our study, the technique of creating data with and without noise showed that the obtained parameters were in line with the proposed ones. In addition, the run of the three field examples from Slovakia, Cuba, and India confirmed the accessibility of our technique to obtain accurate worthy geological or geophysical information.

The method

The gravity anomaly (g) generated by three most popular simple shapes (a sphere, a horizontal cylinder and a semi-infinite vertical cylinder) along the profile is represented as follows (Gupta 1983; Asfahani and Tlas 2015; Tlas and Asfahani 2019):

$$g(x, z, s_n) = \frac{K}{\left[(x - x_o)^2 + z^2\right]^{s_n}}, i = 1, 2, 3, \ldots, N \quad (1)$$

where

$$K = \begin{cases} \frac{4}{3}\pi G\Delta\sigma z R^3 \\ 2\pi G\Delta\sigma z R^2 \\ \pi G\Delta\sigma z R^2 \end{cases}, s_n = \begin{cases} 1.5 \text{ for a sphere model} \\ 1.0 \text{ for a horizontal cylinder model} \\ 0.5 \text{ for a vertical cylinder model} \end{cases}$$

z is the depth, K is the amplitude coefficient, which depends on the shape, s_n is the shape index, x is the location coordinate, x_o is the position of the anomaly central point, $\Delta\sigma$ is the contrast in density between the target structure and the surrounds, G is the universal gravitational constant ($= 6.67 \times 10^{-11}$), and R is the radius of the buried body.

The 2D analytical signal (A_s) of gravity anomaly (Nabighian 1972; Ansari and Alamdar 2010) is:

$$A_s(x, z) = \sqrt{\left(\frac{\partial g}{\partial x}\right)^2 + \left(\frac{\partial g}{\partial z}\right)^2}, \quad (2)$$

where $\frac{\partial g}{\partial x}$ and $\frac{\partial g}{\partial z}$ are the derivatives (horizontal and vertical) of gravity.

By using Eq. (1) and substituting in Eq. (2), the 2D analytical signal of the gravity anomaly is:

$$A_s(x, z) = \frac{2Ks_n}{\left[(x - x_o)^2 + z^2\right]^{s_n + 0.5}}. \quad (3)$$

The horizontal location located under the peak of analytical signal, and the value of $A_s(x_i, z)$ at the horizontal location x_o are given as:

$$A_s(x_o, z) = \frac{2Ks_n}{z^{2s_n + 1}}. \quad (4)$$

Using the normalized equation at $x_i = \pm N$ and $x_i = \pm M$ where N and M are positive integer values (1, 2, 3, …)

$$\frac{A_s(N, z)}{A_s(x_o, z)} = \frac{z^{2s_n + 1}}{\left[(N - x_o)^2 + z^2\right]^{s_n + 0.5}}, \quad (5)$$

$$\frac{A_s(M, z)}{A_s(x_o, z)} = \frac{z^{2s_n + 1}}{\left[(M - x_o)^2 + z^2\right]^{s_n + 0.5}}, \quad (6)$$

Let $F = \frac{A_s(N,z)}{A_s(x_o,z)}$ and $T = \frac{A_s(M,z)}{A_s(x_o,z)}$ then divided Eq. (6) by Eq. (5), we get:

$$\frac{T}{F} = \frac{\left[(N - x_o)^2 + z^2\right]^{s_n + 0.5}}{\left[(M - x_o)^2 + z^2\right]^{s_n + 0.5}} = \left\{\frac{(N - x_o)^2 + z^2}{(M - x_o)^2 + z^2}\right\}^{s_n + 0.5},$$

$$w = \left(\frac{T}{F}\right)^{1/s_n} + 0.5 = \left\{\frac{(N-x_o)^2 + z^2}{(M-x_o)^2 + z^2}\right\}, \text{ and then}$$

$$z = \sqrt{\frac{w(M-x_o)^2 - (N-x_o)^2}{1-w}}, M \neq N \tag{7}$$

Equation (7) can be deciphered for depth utilizing the simple calculation.

For all N and M values (M ≠ N), we estimated the model parameters (z, s_n and K) from Eqs. (7) and (4), correspondingly. For any suggestion for initial guess for z works well for the reason that there was always one solution called a
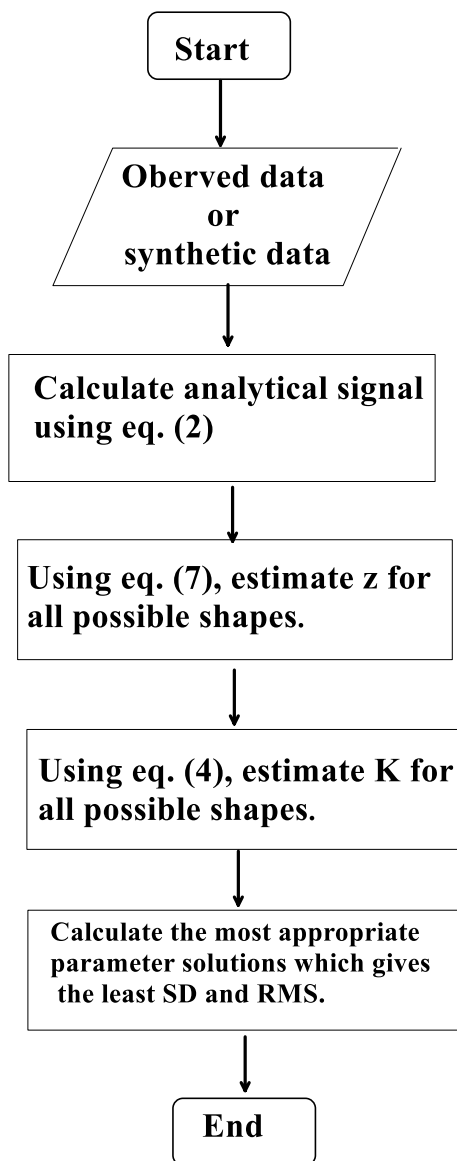

Fig. 2 Noise-free and noisy gravity anomalies of a horizontal cylinder placed at a horizontal distance of 0 m and a depth of 2 m

global minimum solution. Equation (7) was utilized not only to decide z but also to assess s_n of the subsurface structure. Then the standard deviation (SD) of z for each s_n was assessed. The minimum SD is a criterion for defining the true s_n and z of the buried structure. When the true s_n is utilized, the SD of z is continually less than the SD estimated for false s_n. A flow chart (Fig. 1) described this method procedure.

Fig. 1 A flow chart to demonstrate the suggested method works

Fig. 3 Analytical signals of the anomaly in Fig. 2

Table 1 Numerical results of the suggested method applied to the horizontal cylinder model ($K = 100$ mGal$\times$m^2, $z = 2$ m, $s_n = 1$, $x_o = 0$ m, and profile length $= 100$ m) without and with a Gaussian random noise
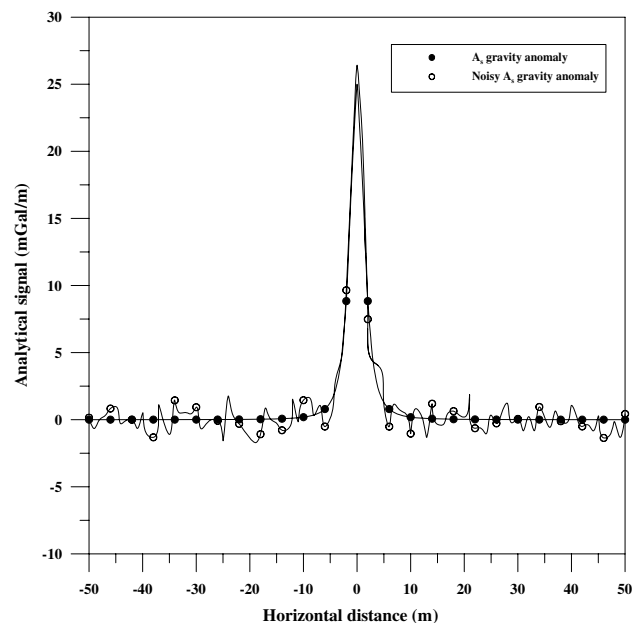
Using noise-free synthetic data

M (m)	N = 1 (m)		N = 2 (m)		N = 3 (m)		N = 4 (m)		N = 5 (m)	
	z_c (m)	K_c (mGal$\times$m^{2sn})	z_c (m)	K_c (mGal$\times$m^{2sn})	z_c (m)	K_c (mGal$\times$m^{2sn})	z_c (m)	K_c (mGal$\times$m^{2sn})	z_c (m)	K_c (mGal$\times$m^{2sn})
In case of using $s_n = 0.5$										
1.00	nc	nc	1.39	48.25	1.23	37.65	1.07	28.57	0.92	21.27
2.00	1.39	48.25	nc	nc	0.82	16.66	0.25	1.60	0.66	11.04
3.00	1.23	37.65	0.82	16.66	nc	nc	1.14	32.32	1.46	53.46
4.00	1.07	28.57	0.25	1.60	1.14	32.32	nc	nc	1.98	98.40
5.00	0.92	21.27	0.66	11.04	1.46	53.46	1.98	98.40	nc	nc
6.00	0.79	15.46	0.93	21.42	1.69	71.50	2.25	126.54	2.69	181.39
7.00	0.66	10.81	1.09	29.92	1.86	86.72	2.46	151.05	2.95	217.03
8.00	0.53	7.04	1.22	36.93	2.00	99.58	2.62	172.27	3.15	248.64
9.00	0.40	3.95	1.31	42.77	2.10	110.49	2.76	190.64	3.33	276.57
10.00	0.23	1.37	1.38	47.68	2.19	119.81	2.87	206.59	3.47	301.24
Average	0.80	19.37	1.01	28.47	1.61	69.80	1.93	112.00	2.29	156.56
SD	0.39	16.04	0.38	16.78	0.48	36.85	0.91	75.98	1.07	112.68
In case of using $s_n = 1.0$										
1.00	nc	nc	2.00	100.00	2.00	100.00	2.00	100.00	2.00	100.00
2.00	2.00	100.00	nc	nc	2.00	100.00	2.00	100.00	2.00	100.00
3.00	2.00	100.00	2.00	100.00	nc	nc	2.00	100.00	2.00	100.00
4.00	2.00	100.00	2.00	100.00	2.00	100.00	nc	nc	2.00	100.00
5.00	2.00	100.00	2.00	100.00	2.00	100.00	2.00	100.00	nc	nc
6.00	2.00	100.00	2.00	100.00	2.00	100.00	2.00	100.00	2.00	100.00
7.00	2.00	100.00	2.00	100.00	2.00	100.00	2.00	100.00	2.00	100.00
8.00	2.00	100.00	2.00	100.00	2.00	100.00	2.00	100.00	2.00	100.00
9.00	2.00	100.00	2.00	100.00	2.00	100.00	2.00	100.00	2.00	100.00
10.00	2.00	100.00	2.00	100.00	2.00	100.00	2.00	100.00	2.00	100.00
Average	**2.00**	**100.00**	**2.00**	**100.00**	**2.00**	**100.00**	**2.00**	**100.00**	**2.00**	**100.00**
SD	**0.00**	**0.00**	**0.00**	**0.00**	**0.00**	**0.00**	**0.00**	**0.00**	**0.00**	**0.00**
In case of using $s_n = 1.5$										
1.00	nc	nc	2.47	309.93	2.58	367.08	2.68	432.45	2.79	502.77
2.00	2.47	309.93	nc	nc	2.72	454.20	2.85	552.65	2.98	661.00
3.00	2.58	367.08	2.72	454.20	nc	nc	3.06	729.16	3.22	898.95
4.00	2.68	432.45	2.85	552.65	3.06	729.16	nc	nc	3.46	1200.94
5.00	2.79	502.77	2.98	661.00	3.22	898.95	3.46	1200.94	nc	nc
6.00	2.88	576.35	3.11	776.60	3.38	1083.95	3.65	1481.72	3.92	1958.03
7.00	2.97	652.23	3.22	897.81	3.52	1281.42	3.83	1786.31	4.12	2399.77
8.00	3.06	729.84	3.33	1023.53	3.66	1489.36	3.99	2111.51	4.31	2877.10
9.00	3.14	808.79	3.43	1152.98	3.78	1706.29	4.14	2454.82	4.49	3386.20
10.00	3.21	888.82	3.52	1285.59	3.90	1931.05	4.29	2814.18	4.66	3923.91
Average	2.87	585.36	3.07	790.48	3.31	1104.61	3.55	1507.08	3.77	1978.74
SD	0.26	200.36	0.35	327.85	0.46	544.86	0.58	852.59	0.68	1246.76
Using noisy synthetic data										
In case of using $s_n = 0.5$										
1.00	nc	nc	1.54	62.05	1.50	58.91	0.82	17.38	1.11	32.25
2.00	2.12	120.88	nc	nc	1.42	52.77	1.10	31.50	0.17	0.71
3.00	2.11	120.33	1.42	52.77	nc	nc	2.30	138.38	1.52	60.53
4.00	1.41	35.68	1.10	31.50	2.30	138.38	nc	nc	6.00	939.57

Table 1 (continued)

Using noise-free synthetic data

M (m)	N = 1 (m)		N = 2 (m)		N = 3 (m)		N = 4 (m)		N = 5 (m)	
	z_c (m)	K_c (mGal $\times$ m^{2sn})	z_c (m)	K_c (mGal $\times$ m^{2sn})	z_c (m)	K_c (mGal $\times$ m^{2sn})	z_c (m)	K_c (mGal $\times$ m^{2sn})	z_c (m)	K_c (mGal $\times$ m^{2sn})
5.00	0.47	1.29	0.17	0.71	1.52	60.53	6.00	939.57	nc	nc
6.00	3.16	402.13	2.15	120.08	2.85	211.36	14.11	5193.51	8.41	1844.51
7.00	1.00	12.73	2.09	113.72	2.66	184.65	12.05	3785.26	29.33	22,433.83
8.00	1.00	12.73	0.56	8.14	1.14	34.08	3.23	272.41	1.69	74.55
9.00	4.33	1035.08	3.19	265.42	4.35	493.21	6.04	953.05	6.68	1165.39
10.00	1.00	12.73	0.83	17.94	0.72	13.66	3.39	300.02	2.35	144.33
Average	1.84	194.84	1.45	74.70	2.05	138.62	5.45	1292.34	6.36	2966.19
SD	1.24	339.54	0.93	83.36	1.11	149.79	4.73	1879.00	9.08	7329.45
In case of using $s_n = 1.0$										
1.00	nc	nc	2.12	120.88	2.11	120.33	1.84	93.56	2.14	100.29
2.00	1.98	97.04	nc	nc	2.11	119.52	1.93	100.74	1.92	104.54
3.00	2.12	103.62	2.11	119.52	nc	nc	2.04	107.85	2.16	112.79
4.00	2.07	101.37	1.93	100.74	2.04	107.85	nc	nc	2.05	109.95
5.00	2.04	99.79	1.92	104.52	2.02	107.79	2.05	104.95	nc	nc
6.00	2.32	113.73	2.14	112.91	2.05	105.21	2.03	10.3.77	2.13	107.51
7.00	1.99	99.45	2.00	101.85	2.01	103.74	2.00	101.79	2.00	105.91
8.00	2.23	111.44	2.00	101.85	1.96	98.98	2.00	102.14	2.05	109.14
9.00	2.12	105.79	1.94	95.95	2.14	105.37	2.14	108.78	2.10	102.55
10.00	2.31	115.26	2.00	101.85	2.12	103.41	2.00	105.12	2.00	103.91
Average	**2.13**	**105.28**	**2.02**	**106.67**	**2.06**	**108.02**	**2.00**	**103.12**	**2.06**	**106.29**
SD	**0.13**	**6.70**	**0.08**	**8.88**	**0.06**	**7.25**	**0.08**	**4.80**	**0.08**	**3.94**
In case of using $s_n = 1.5$										
1.00	nc	nc	2.45	294.77	2.15	177.15	3.26	926.87	2.26	216.19
2.00	4.51	2219.50	nc	nc	1.80	85.66	3.99	2079.88	2.14	174.49
3.00	5.02	3058.83	2.15	177.15	nc	nc	11.94	167,521.90	2.54	345.76
4.00	5.23	3458.92	3.26	926.87	11.94	167,521.70	nc	nc	2.85	547.38
5.00	5.98	5194.92	2.26	216.19	2.54	345.76	2.85	547.38	nc	nc
6.00	5.67	4407.81	3.31	985.14	5.84	9615.93	3.46	1177.04	8.93	52,508.14
7.00	6.17	5686.44	2.75	470.57	3.75	1637.15	1.23	19.11	6.70	16,617.89
8.00	6.48	6595.32	4.92	4841.97	10.70	108,196.30	8.68	46,891.90	12.64	210,319.30
9.00	6.70	7274.12	1.00	8.24	3.00	667.71	4.00	2110.29	5.00	5152.06
10.00	8.08	12,806.48	2.99	656.18	4.09	2306.23	2.48	314.24	5.99	10,643.01
Average	5.98	5633.59	2.79	953.01	5.09	32,283.73	4.66	24,620.96	5.45	32,947.14
SD	1.06	3157.91	1.07	1496.55	3.74	61,736.21	3.41	55,698.00	3.57	68,591.32

nc is not converge

Bold indicates the true average values at the minimum SD

Application to synthetic examples

First model

A noise-free gravity anomaly profile of a horizontal cylinder model of parameters: $K = 100$ mGal $\times$ m^2, $z = 2$ m, $s_n = 1$, $x_o = 0$ m, and profile length $= 100$ m was chosen (as shown in Fig. 2). The model equation is:

$$g(x) = \frac{100}{\left[(x-0)^2 + 2^2\right]^1} \tag{8}$$

By using the Fourier transform method, the horizontal and vertical derivatives of gravity anomaly and then the analytic signal of the data were estimated (Fig. 3). The new technique was utilized to the gravity anomaly profile and inverted to retrieve the target parameters; the depth (z), the shape index (s_n) and the
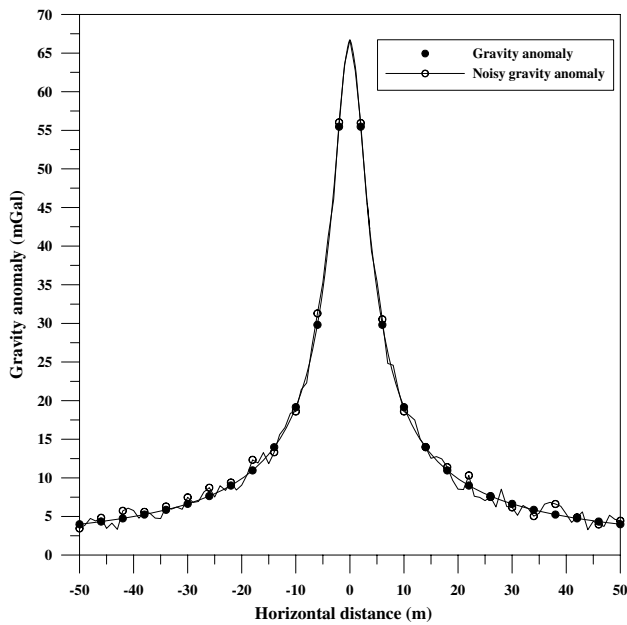
Fig. 4 Noise-free and noisy gravity anomalies of a semi-infinite vertical cylinder located at a horizontal distance of 0 m and a depth of 3 m
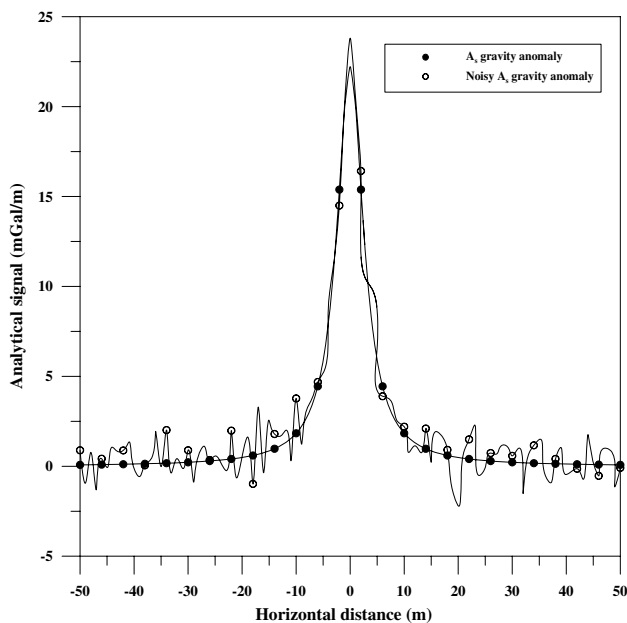

Fig. 5 Analytical signals of the anomaly in Fig. 4

amplitude coefficient (K), correspondingly. The solutions for all combination of N and M points were found valid.

Table 1 displays the effect of different N and M values, i.e., for $N = 1, 2, 3, 4$, and 5 m and $M = 1, 2, 3,…, 10$ m. The

computed model parameters also were explained in Table 1. It displays the model parameters (z, s_n, K), in cases of using $s_n = 0.5$, 1.0, and $s_n = 1.5$. The correct solution was valid at the minimum SD, which occurs at $s_n = 1.0$. So, the method was deemed to be convergent at the correct solutions. Therefore, noise-free data were inferred to authenticate the effectiveness of the method in deducing the actual model parameters.

The above-mentioned synthetic data was infected with Gaussian noise (with standard deviation = 1 and mean = 0) to examine the stability of the suggested method. The estimated model parameters were presented in Table 1 for all suggested N and M values mentioned-above. Furthermore, Table 1 also indicates the model parameter solutions (z, s_n, K), in all cases of using $s_n = 0.5$, 1.0, and 1.5. The acceptable solution was seen at the lowest SD, which occurred in $s_n = 1.0$ (Table 1). Finally, the method was convergent with the correct solutions even when the data contained a noise.

Second model

A noise-free gravity anomaly profile of a semi-infinite vertical cylinder model with K = 200 mGal × m, z = 3 m, $s_n = 0.5$, $x_o = 0$ m, and profile length = 100 m (Fig. 4) was adopted. The model equation is:

$$g(x) = \frac{200}{\left[(x - 0)^2 + 3^2\right]^{0.5}} \tag{9}$$

By using the Fourier transform, the horizontal and vertical derivatives of the gravity anomaly and then the analytic signal of the data could be estimated (Fig. 5).

The suggested technique was used to the gravity anomaly profile and inverted to recover the parameters; the depth (z), the shape index (s_n) and the amplitude coefficient (K), respectively (Table 2). Table 2 indicates the solutions for all estimated parameters applying various combinations of N and M points through using different s_n values ($s_n = 0.5$, 1.0, and $s_n = 1.5$). The true-values of the parameters are valid at the SD minima, which happens at $s_n = 0.5$ (Table 2).

The above-mentioned generated synthetic data applying Eq. (9) was then contaminated with Gaussian noise (with standard deviation = 1 and mean = 0) (Fig. 4). For the same combination of N and M values, the estimated model parameters were offered in Table 2. Table 2 indicates that the model parameters estimation (z, s_n, K) in the case of using $s_n = 0.5$ were acceptable because they had the lowest SD.

Table 2 Numerical results of the suggested method applied to the semi-vertical cylinder model (K = 200 mGal × m, z = 3 m, s_n = 0.5, x_o = 0 m, and profile length = 100 m) without and with a Gaussian random noise

M (m)	N=1 (m) z_c (m)	N=1 (m) K_c (mGal×m^{2sn})	N=2 (m) z_c (m)	N=2 (m) K_c (mGal×m^{2sn})	N=3 (m) z_c (m)	N=3 (m) K_c (mGal×m^{2sn})	N=4 (m) z_c (m)	N=4 (m) K_c (mGal×m^{2sn})	N=5 (m) z_c (m)	N=5 (m) K_c (mGal×m^{2sn})
Using noise-free synthetic data										
In case of using s_n = 0.5										
1.00	nc	nc	3.00	200.00	3.00	200.00	3.00	200.00	3.00	200.00
2.00	3.00	200.00	nc	nc	3.00	200.00	3.00	200.00	3.00	200.00
3.00	3.00	200.00	3.00	200.00	nc	nc	3.00	200.00	3.00	200.00
4.00	3.00	200.00	3.00	200.00	3.00	200.00	nc	nc	3.00	200.00
5.00	3.00	200.00	3.00	200.00	3.00	200.00	3.00	200.00	nc	nc
6.00	3.00	200.00	3.00	200.00	3.00	200.00	3.00	200.00	3.00	200.00
7.00	3.00	200.00	3.00	200.00	3.00	200.00	3.00	200.00	3.00	200.00
8.00	3.00	200.00	3.00	200.00	3.00	200.00	3.00	200.00	3.00	200.00
9.00	3.00	200.00	3.00	200.00	3.00	200.00	3.00	200.00	3.00	200.00
10.00	3.00	200.00	3.00	200.00	3.00	200.00	3.00	200.00	3.00	200.00
Average	**3.00**	**200.00**	**3.00**	**200.00**	**3.00**	**200.00**	**3.00**	**200.00**	**3.00**	**200.00**
SD	**0.00**	**0.00**	**0.00**	**0.00**	**0.00**	**0.00**	**0.00**	**0.00**	**0.00**	**0.00**
In case of using s_n = 1.0										
1.00	nc	nc	3.83	625.94	3.96	689.63	4.10	766.09	4.25	850.72
2.00	3.83	625.94	nc	nc	4.08	754.02	4.24	845.74	4.40	947.84
3.00	3.96	689.63	4.08	754.02	nc	nc	4.43	963.46	4.62	1092.27
4.00	4.10	766.09	4.24	845.74	4.43	963.46	nc	nc	4.85	1270.49
5.00	4.25	850.72	4.40	947.84	4.62	1092.27	4.85	1270.49	nc	nc
6.00	4.39	940.76	4.56	1056.99	4.80	1230.87	5.07	1446.82	5.34	1693.77
7.00	4.53	1034.53	4.72	1171.17	4.99	1376.67	5.28	1633.36	5.58	1928.55
8.00	4.67	1130.97	4.88	1289.06	5.16	1527.95	5.48	1827.92	5.81	2174.60
9.00	4.80	1229.40	5.02	1409.80	5.33	1683.58	5.67	2028.95	6.02	2429.92
10.00	4.93	1329.36	5.17	1532.80	5.49	1842.72	5.86	2235.35	6.23	2693.02
Average	4.38	955.27	4.55	1070.37	4.76	1240.13	5.00	1446.46	5.23	1675.69
SD	0.38	244.49	0.45	306.25	0.54	402.97	0.64	527.98	0.73	673.79
In case of using s_n = 1.5										
1.00	nc	nc	4.52	3083.20	4.73	3722.19	4.98	4560.04	5.24	5577.06
2.00	4.52	3083.20	nc	nc	4.93	4372.94	5.20	5411.11	5.48	6677.25
3.00	4.73	3722.19	4.93	4372.94	nc	nc	5.50	6761.76	5.81	8431.82
4.00	4.98	4560.04	5.20	5411.11	5.50	6761.76	nc	nc	6.18	10,783.60
5.00	5.24	5577.06	5.48	6677.25	5.81	8431.82	6.18	10,783.59	nc	nc
6.00	5.50	6761.76	5.76	8158.24	6.12	10,394.74	6.52	13,405.47	6.94	17,148.70
7.00	5.75	8107.39	6.04	9846.40	6.43	12,641.47	6.86	16,417.92	7.31	21,128.37
8.00	6.00	9609.88	6.31	11,737.08	6.73	15,166.55	7.19	19,814.52	7.67	25,627.82
9.00	6.24	11,266.67	6.57	13,827.37	7.02	17,966.57	7.51	23,591.21	8.02	30,642.30
10.00	6.48	13,076.09	6.83	16,115.37	7.30	21,039.26	7.82	27,745.38	8.36	36,168.77
Average	5.49	7307.14	5.74	8803.22	6.06	11,166.37	6.42	14,276.78	6.78	18,020.63
SD	0.68	3471.89	0.78	4432.74	0.90	6030.49	1.03	8260.34	1.15	11,094.95
Using noisy synthetic data										
In case of using s_n = 0.5										
1.00	nc	nc	2.88	183.63	3.09	211.04	3.00	198.67	2.94	189.00
2.00	3.18	222.09	nc	nc	3.34	246.66	3.08	208.96	2.83	175.00
3.00	2.93	188.66	3.34	246.66	nc	nc	2.75	167.11	2.94	189.60
4.00	2.95	191.26	3.08	208.96	2.75	267.11	nc	nc	2.84	176.25

Table 2 (continued)

Using noise-free synthetic data

M (m)	N = 1 (m)		N = 2 (m)		N = 3 (m)		N = 4 (m)		N = 5 (m)	
	z_c (m)	K_c (mGal × m^{2sn})	z_c (m)	K_c (mGal × m^{2sn})	z_c (m)	K_c (mGal × m^{2sn})	z_c (m)	K_c (mGal × m^{2sn})	z_c (m)	K_c (mGal × m^{2sn})
5.00	2.94	189.00	2.84	177.83	2.46	233.78	2.88	183.63	nc	nc
6.00	2.99	195.61	3.16	220.99	3.06	206.78	3.09	211.04	3.50	267.79
7.00	3.15	217.91	3.34	246.03	3.34	245.72	3.00	198.67	3.21	227.25
8.00	3.32	242.17	2.73	164.13	2.42	129.57	2.85	179.78	2.77	169.54
9.00	3.02	199.74	3.57	281.21	3.66	296.15	3.08	209.17	3.34	243.81
10.00	3.10	210.91	2.39	126.05	3.39	253.73	3.15	218.06	3.11	211.36
Average	**3.07**	**206.37**	**3.04**	**206.16**	**3.06**	**210.06**	**2.99**	**197.23**	**3.05**	**205.51**
SD	**0.13**	**18.32**	**0.36**	**48.20**	**0.43**	**57.10**	**0.13**	**16.98**	**0.25**	**34.39**
In case of using $s_n = 1.0$										
1.00	nc	nc	3.92	663.98	3.80	605.05	4.00	705.56	4.32	888.05
2.00	3.92	663.98	nc	nc	3.70	557.47	4.04	726.39	4.47	981.70
3.00	3.80	605.05	3.70	557.47	nc	nc	4.49	998.70	5.05	1422.98
4.00	4.00	705.56	4.04	726.39	4.49	998.70	nc	nc	5.83	2184.22
5.00	4.32	888.05	4.47	981.70	5.05	1422.98	5.83	2184.22	nc	nc
6.00	4.60	1075.18	4.81	1228.81	5.45	1783.41	6.18	2598.56	6.60	3173.14
7.00	4.22	826.36	4.29	872.99	4.56	1045.23	4.60	1069.22	3.87	636.25
8.00	4.73	1165.10	4.92	1315.42	5.41	1748.90	5.81	2163.37	5.80	2153.99
9.00	5.00	1379.00	5.25	1590.08	5.81	2160.18	6.31	2766.39	6.49	3009.11
10.00	5.25	1597.08	5.54	1868.90	6.16	2572.07	6.73	3356.07	7.02	3815.14
Average	4.43	989.48	4.55	1089.53	4.94	1432.66	5.33	1840.94	5.49	2029.40
SD	0.50	341.02	0.62	444.83	0.86	692.82	1.05	986.41	1.12	1129.45
In case of using $s_n = 1.5$										
1.00	nc	nc	4.32	2573.35	4.84	4021.07	4.98	4511.19	5.19	5330.62
2.00	4.32	2573.35	nc	nc	5.36	6083.22	5.31	5833.17	5.50	6712.60
3.00	4.84	4021.07	5.36	6083.23	nc	nc	5.25	5600.36	5.57	7061.42
4.00	4.98	4511.19	5.31	5833.18	5.25	5600.35	nc	nc	5.94	9182.62
5.00	5.19	5330.62	5.50	6712.60	5.57	7061.42	5.94	9182.61	nc	nc
6.00	5.64	7455.37	6.03	9723.22	6.29	11,538.21	7.03	17,965.50	8.61	40,450.47
7.00	5.69	7720.40	6.03	9720.12	6.24	11,130.02	6.71	14,937.47	7.23	20,091.24
8.00	5.98	9385.44	6.34	11,899.31	6.61	14,011.84	7.14	19,133.92	7.73	26,232.12
9.00	6.23	11,102.00	6.62	14,125.74	6.92	16,905.22	7.49	23,193.86	8.11	31,767.75
10.00	6.60	13,938.92	7.03	17,961.34	7.40	22,071.58	8.06	31,070.69	8.79	43,935.59
Average	5.50	7337.59	5.84	9403.56	6.05	10,935.88	6.44	14,603.20	6.96	21,196.05
SD	0.73	3671.11	0.81	4738.55	0.85	5961.76	1.10	9124.95	1.43	15,131.74

nc is not converge

Bold indicates the true average values at the minimum SD

Therefore, it was evident that the assessed parameters reflected the stability and efficiency of the suggested method in interpreting the gravity data.

Third model

A gravity anomaly profile of a sphere model with K = 150 mGal × m^3, z = 5 m, s_n = 1.5, x_o = 0 m, and length = 100 m (Fig. 6) was adopted. The model equation is:
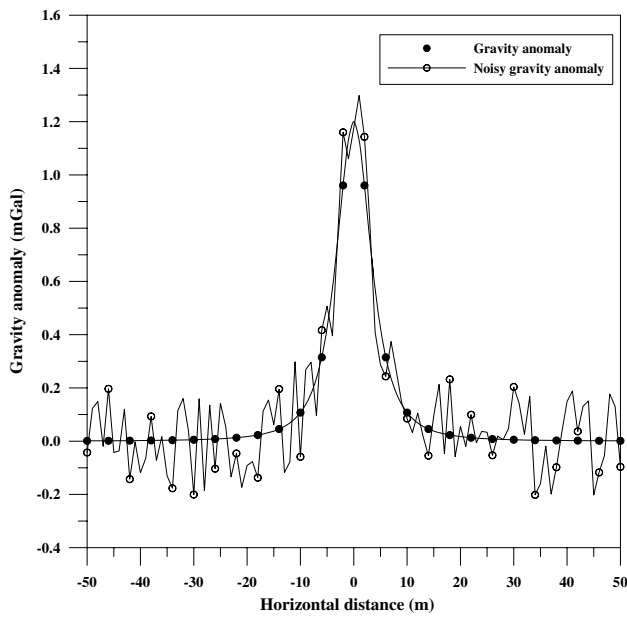
Fig. 6 Noise-free and noisy gravity anomalies of a sphere located at a horizontal distance of 0 m and a depth of 5 m
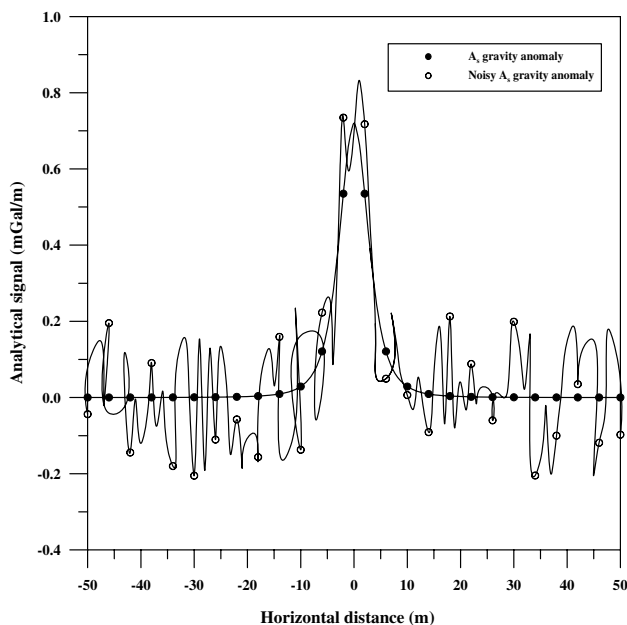

Fig. 7 Analytical signals of the anomaly in Fig. 6

$$g(x) = \frac{150}{\left[(x-0)^2 + 5^2\right]^{1.5}}. \tag{10}$$

By using the Fourier transform, the horizontal and vertical derivatives of the gravity anomaly and then the analytic signal of the data were estimated (Fig. 7).

The suggested technique was applied to this anomaly profile without and including Gaussian noise (with standard deviation = 1 and mean = 0) (Fig. 6) and inverted to recover the model parameters (Table 3). Table 3 explains the percentage of errors in z and K for all available combination N and M values using $s_n = 1.5$.

So, the percentage of error in z and K was zero in the noise-free case. However, in the noisy case, the maximum error in z and K were 9.6% and 10.1% respectively.

Fourth model

A forward gravity response of three different anomalies consisted of a *sphere* model whose model parameters were K = 10,000 mGal × m³, z = 7 m, $s_n = 1.5$ and $x_o = 15$ m, a *horizontal* cylinder whose model parameters is K = 100 mGal × m², z = 3 m, $s_n = 1$ and $x_o = 50$ m, and a *horizontal* cylinder whose model parameter is K = 50 mGal × m², z = 1 m, $s_n = 1$, and $x_o = 70$ m (Fig. 8). Adapting the same procedures mentioned-above, the Analytical signal was created as shown in Fig. 9.

The new method was applied to the gravity response profile and inverted to retrieve the model parameters; z, s_n and K, individually, to validate the outcomes for all combinations of N and M points. The estimated parameters are presented in Fig. 10 which demonstrates that the method converges at the correct solutions (z, s_n) for every model. This is evident of the fact that suitable inversion outcomes were achieved by employing the new current algorithm specifically for depth and shape index, which is a targeted concern in gravity exploration for minerals which have an economic significance.

Effect of choosing x_o

It was well known that incorrect estimation of the origin of buried structures causes an error in model parameters estimation while inferring the real data. Since we were attempting to study the effect of choosing the wrong origin (x_o) as stated in Eq. (9), the origin of the horizontal cylinder model (K = 100 mGal × m², z = 2 m, $s_n = 1$, $x_o = 0$ m, and profile length = 100 m) was anticipated to be picked incorrectly by introducing errors of $0, \pm 0.2, \pm 4, \ldots, \pm 1.0$ m in the horizontal coordinate x_i.

After the similar elucidation method applied, the results were revealed in Fig. 11which shows that the error in model parameters appraised increases with increasing error in x_o. This demonstrates that the determination of x_o is very significant in our method.

Table 3 Numerical results of the suggested method applied to the sphere model ($K = 150$ mGal$\times$m^3, $z = 5$ m, $s_n = 1.5$, $x_o = 0$ m, and profile length $= 100$ m) without and with a Gaussian random noise

N (m)	M (m)	Using noise-free synthetic data		Using noisy synthetic data	
		Error in depth, z (%)	Error in Amplitude coefficient, K (%)	Error in depth, z (%)	Error in Amplitude coefficient, K (%)
1.00	1.00	nc	nc	nc	nc
1.00	2.00	0.00	0.00	− 2.86	− 6.61
1.00	3.00	0.00	0.00	2.63	3.15
1.00	4.00	0.00	0.00	− 3.98	− 8.29
1.00	5.00	0.00	0.00	9.70	6.11
1.00	6.00	0.00	0.00	6.74	4.80
1.00	7.00	0.00	0.00	8.72	7.05
1.00	8.00	0.00	0.00	4.59	4.54
1.00	9.00	0.00	0.00	− 8.00	− 9.98
1.00	10.00	0.00	0.00	4.81	4.13
2.00	1.00	0.00	0.00	− 2.86	− 6.61
2.00	2.00	nc	nc	nc	nc
2.00	3.00	0.00	0.00	− 5.87	− 9.62
2.00	4.00	0.00	0.00	− 7.89	− 9.97
2.00	5.00	0.00	0.00	3.83	5.30
2.00	6.00	0.00	0.00	1.78	1.64
2.00	7.00	0.00	0.00	6.00	7.65
2.00	8.00	0.00	0.00	1.10	2.29
2.00	9.00	0.00	0.00	− 6.00	− 9.67
2.00	10.00	0.00	0.00	7.52	8.01
3.00	1.00	0.00	0.00	2.63	3.15
3.00	2.00	0.00	0.00	− 5.87	− 9.62
3.00	3.00	nc	nc	nc	nc
3.00	4.00	0.00	0.00	− 6.81	− 9.86
3.00	5.00	0.00	0.00	4.41	6.20
3.00	6.00	0.00	0.00	1.61	2.01
3.00	7.00	0.00	0.00	1.94	2.96
3.00	8.00	0.00	0.00	1.08	1.55
3.00	9.00	0.00	0.00	− 4.00	− 8.31
3.00	10.00	0.00	0.00	2.39	3.11
4.00	1.00	0.00	0.00	− 3.98	− 8.29
4.00	2.00	0.00	0.00	− 7.89	− 9.97
4.00	3.00	0.00	0.00	− 6.81	− 9.86
4.00	4.00	nc	nc	nc	nc
4.00	5.00	0.00	0.00	0.75	7.38
4.00	6.00	0.00	0.00	3.74	6.50
4.00	7.00	0.00	0.00	5.96	7.46
4.00	8.00	0.00	0.00	9.22	10.01
4.00	9.00	0.00	0.00	− 2.00	− 4.66
4.00	10.00	0.00	0.00	5.92	7.94
5.00	1.00	0.00	0.00	9.70	10.11
5.00	2.00	0.00	0.00	9.38	10.10
5.00	3.00	0.00	0.00	4.41	6.20
5.00	4.00	0.00	0.00	0.75	7.38
5.00	5.00	nc	nc	nc	nc
5.00	6.00	0.00	0.00	1.22	2.67
5.00	7.00	0.00	0.00	5.91	8.85

Table 3 (continued)

N (m)	M (m)	Using noise-free synthetic data		Using noisy synthetic data	
		Error in depth, z (%)	Error in Amplitude coefficient, K (%)	Error in depth, z (%)	Error in Amplitude coefficient, K (%)
5.00	8.00	0.00	0.00	1.72	2.54
5.00	9.00	0.00	0.00	0.00	3.03
5.00	10.00	0.00	0.00	2.75	3.79
6.00	1.00	0.00	0.00	2.74	3.80
6.00	2.00	0.00	0.00	1.78	2.64
6.00	3.00	0.00	0.00	1.61	2.01
6.00	4.00	0.00	0.00	3.74	6.50
6.00	5.00	0.00	0.00	1.22	5.67
6.00	6.00	nc	nc	nc	nc
6.00	7.00	0.00	0.00	2.42	3.52
6.00	8.00	0.00	0.00	4.07	7.39
6.00	9.00	0.00	0.00	2.00	7.02
6.00	10.00	0.00	0.00	0.10	1.26
7.00	1.00	0.00	0.00	7.72	8.05
7.00	2.00	0.00	0.00	6.00	7.79
7.00	3.00	0.00	0.00	1.94	2.96
7.00	4.00	0.00	0.00	5.96	7.46
7.00	5.00	0.00	0.00	5.91	8.92
7.00	6.00	0.00	0.00	2.42	3.52
7.00	7.00	nc	nc	nc	nc
7.00	8.00	0.00	0.00	0.48	0.71
7.00	9.00	0.00	0.00	4.00	4.07
7.00	10.00	0.00	0.00	5.90	7.29
8.00	1.00	0.00	0.00	4.59	5.53
8.00	2.00	0.00	0.00	1.10	2.29
8.00	3.00	0.00	0.00	1.83	2.55
8.00	4.00	0.00	0.00	7.22	8.01
8.00	5.00	0.00	0.00	1.72	4.54
8.00	6.00	0.00	0.00	6.07	7.41
8.00	7.00	0.00	0.00	0.48	0.71
8.00	8.00	nc	nc	nc	nc
8.00	9.00	0.00	0.00	6.00	7.41
8.00	10.00	0.00	0.00	1.31	5.72
9.00	1.00	0.00	0.00	3.46	7.40
9.00	2.00	0.00	0.00	1.59	2.60
9.00	3.00	0.00	0.00	4.19	6.88
9.00	4.00	0.00	0.00	5.84	8.99
9.00	5.00	0.00	0.00	8.00	9.93
9.00	6.00	0.00	0.00	1.01	3.58
9.00	7.00	0.00	0.00	8.00	9.93
9.00	8.00	0.00	0.00	6.80	7.93
9.00	9.00	nc	nc	nc	nc
9.00	10.00	0.00	0.00	5.80	6.93
10.00	1.00	0.00	0.00	4.81	7.15
10.00	2.00	0.00	0.00	1.52	3.01
10.00	3.00	0.00	0.00	3.39	4.11
10.00	4.00	0.00	0.00	3.92	5.94

Table 3 (continued)

N (m)	M (m)	Using noise-free synthetic data		Using noisy synthetic data	
		Error in depth, z (%)	Error in Amplitude coefficient, K (%)	Error in depth, z (%)	Error in Amplitude coefficient, K (%)
10.00	5.00	0.00	0.00	2.75	3.79
10.00	6.00	0.00	0.00	2.10	3.26
10.00	7.00	0.00	0.00	5.90	7.29
10.00	8.00	0.00	0.00	1.31	2.72
10.00	9.00	0.00	0.00	1.00	1.52
10.00	10.00	nc	nc	nc	nc

nc is not converge

Fig. 8 A gravity anomaly of three different models which are a sphere situated at a horizontal distance of 15 m and a depth of 7 m, a horizontal cylinder located at a horizontal distance of 50 m and a depth of 3 m, and a horizontal cylinder located at a horizontal distance of 70 m and a depth of 1 m
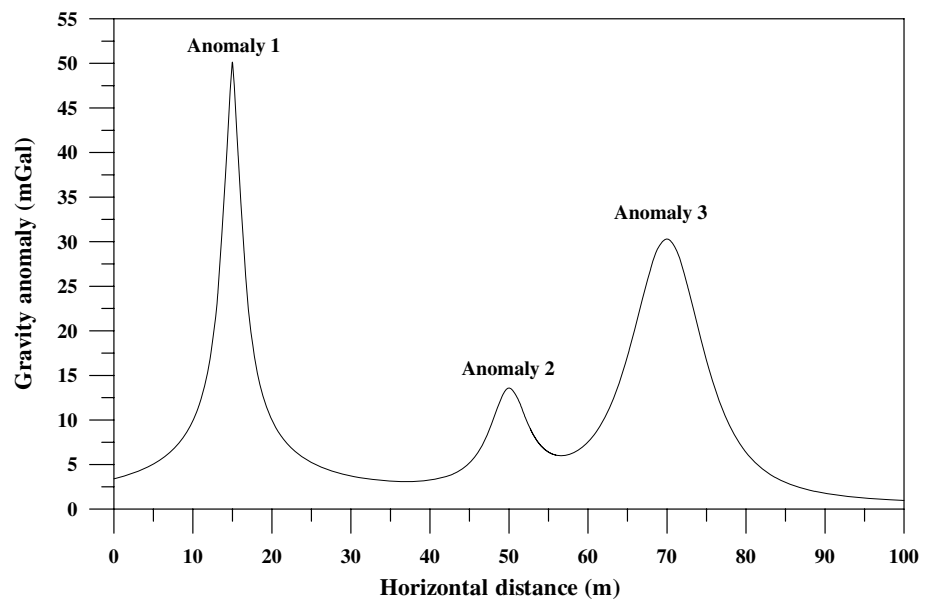
Fig. 9 Analytical signal of the anomalies in Fig. 8
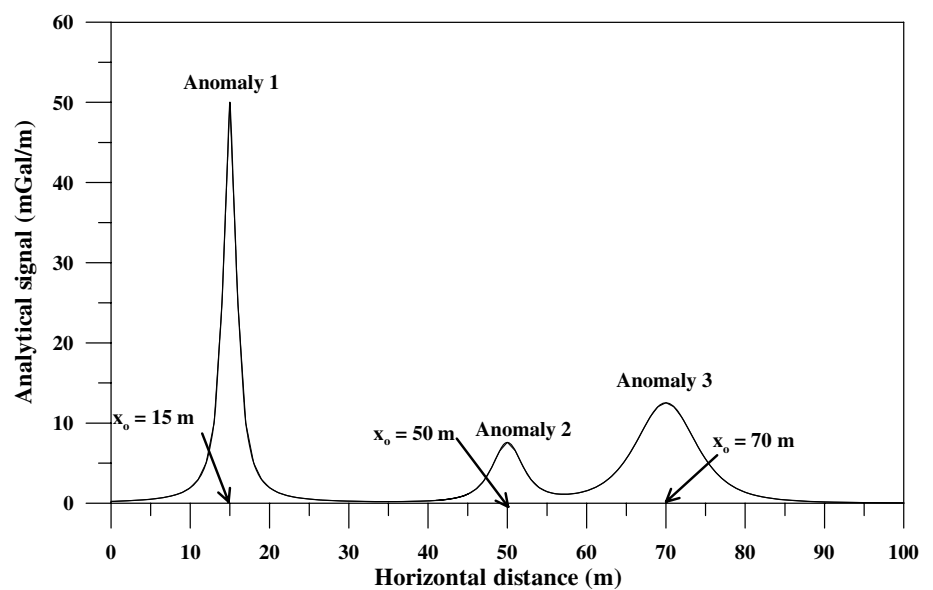
Fig. 10 Numerical results by using the present method for interpreting anomalies in Fig. 9
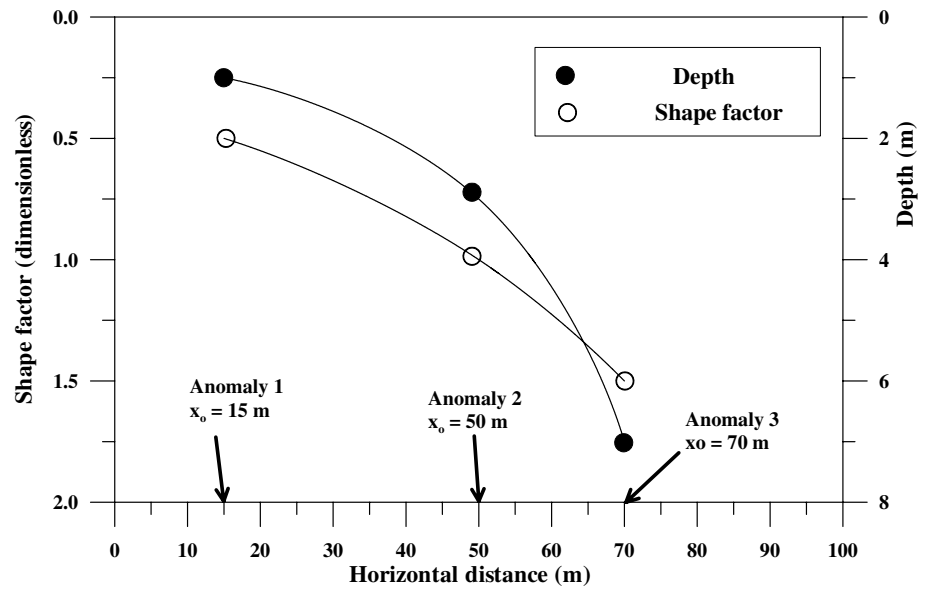
Application to field examples

The proposed method explained in this study was ready and adjusted to investigate the residual gravity anomalies to simple bodies of various structures, e.g., vertical cylinders, spheres, and horizontal cylinders. Three field examples from Slovakia, Cuba and India were re-interpreted to examine the robustness and constancy of the suggested method. The pertinent parameters (K, z, and s_n) were inferred in an integrated manner with the existing geological and geophysical outcomes.

Catholic Church Crypt, Slovakia

As it is argued for not using destructive tools during the exploring process for the archaeological buildings, the proper tool of using the microgravity technique appears on the ground. A good example of using such a technique is the Roman-Catholic Church crypt of St. Nicolas in Pukanec town. This crypt was detected and delineated for its local density variations which had been caused by a near-surface cavity. Microgravity measurements were taken on a 10 m × 20 m grid with a 1 m spacing "somewhere the spacing was less than 1 m due to restrictions on the study area" (Fig. 12). Microgravity data measuring and processing have been examined in detail in past studies (Panisova and Pasteka, 2009).

For further interpretation, the method suggested in our study can be used on the final residual Bouguer anomaly profile (Fig. 13) with negative anomaly amplitude exceeding –30 up to –40μGal. To detect and interpret the existing negative gravity anomaly and estimate the model parameters of the buried anomaly source. The negative residual Bouguer anomaly profile was digitized with an interval of 0.5 m. These digitized residual anomaly profile data were subjected to our new algorithm to achieve the prospected depth, amplitude coefficient, and shape of the buried target anomaly as shown in Table 4.

Table 4 shows the optimum parameters, least SD, $z = 2.08$ m, and $k = -7.66$ mGal × m². The acceptable fit between the observed gravity anomaly over a crypt, St. Nicolas Church, Slovakia (black circles) and calculated
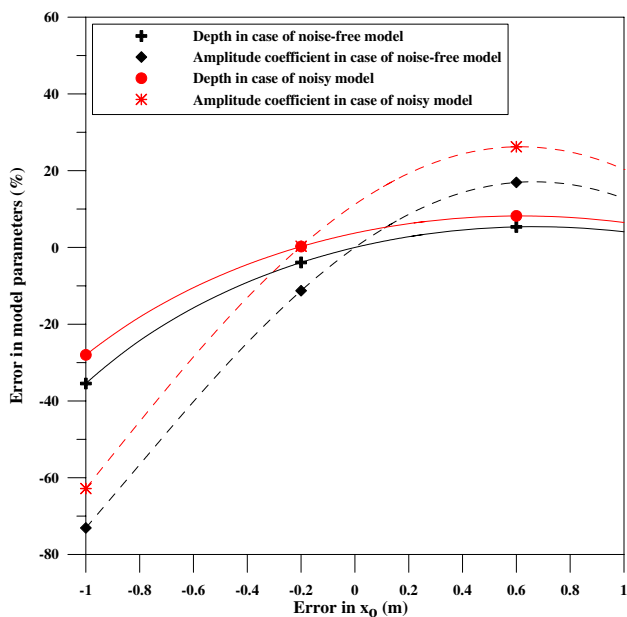
Fig. 11 Error in model parameters estimated after imposing error in x_o in case of noise-free and noisy model mentioned in Fig. 2

Fig. 12 The St. Nicolas church view and a location of the study area in Pukanec-city, southern central Slovakia

gravity anomaly from the present method (open circles) was achieved with a least SD (Fig. 13) and the analytical signal of these gravity data is shown in Fig. 14. The discrepancy between the observed and calculated fields in some places is shown in Fig. 13. Explanations for this can refer to the inadequacy in identifying the corrections of the building influence or the deformation of the residual anomaly field. In addition, Fig. 13 depicts that the crypt could be situated approximately 1 m to the crypt top and 2.08 m depth to the center of the crypt.

Chromite deposit body

Davis et al. (1957) declared that the chromite deposits in the Camagüey Area, Cuba are initiated in complex geological environs including serpentinized peridotite and dunite with little quantities of gabbro, troctolite, and anothosite. The geologic complex environs are seen inhibited into metamorphic rocks and superimposed by upper Cretaceous volcanic rocks with limestone and radiolarian cherts. Chromite is a black, hard moderately heavy mineral that varies widely in

Table 4 Numerical results of the present method applied to a crypt, St. Nicolas Church, Slovakia

M (m)	$s_n = 0.5$		$s_n = 1.0$		$s_n = 1.5$	
	Estimated depth (m)	Estimated amplitude coeff (mGal × m)	Estimated depth (m)	Estimated amplitude coeff (mGal × m^2)	Estimated depth (m)	Estimated amplitude coeff (mGal × m^3)
1.00	1.69	− 6.18	2.14	− 16.83	2.51	− 36.00
1.50	1.85	− 6.82	2.61	− 25.01	3.07	− 65.18
2.00	2.12	− 7.80	2.14	− 16.83	3.77	− 36.00
2.50	2.25	− 8.29	3.20	− 37.72	3.37	− 120.74
3.00	2.50	− 9.21	3.05	− 34.32	4.47	− 104.78
Average	**2.08**	**− 7.66**	2.63	− 26.14	3.44	− 72.54
SD	**0.32**	**1.19**	0.50	9.69	0.74	39.01

Bold indicates the true average values at the minimum SD

composition. The chromites of this area have an average composition and occur as anhedral or occasionally subhedral grains, commonly in a region millimeter or less. They are disseminated principally in dunite and less commonly in peridotite, troctolite, or anorthosite, and as larger masses but all within the peridotite zone although surrounded by a dunite envelope. The texture ranges from that of a normal rock through increasing proportions of chromite and an increase

Fig. 13 Upper panel: The misfit between the observed and calculated data. Middle panel: The measured gravity anomaly (black circles) over a crypt, St. Nicolas Church, Slovakia and the fitted response (open circles) computed from the present method. Bottom panel: Geologic sketch for the crypt from the present method and Panisova and Pasteka method (2009)

in grain size to a massive, moderately coarse-grained aggregate consisting entirely of chromite (Flint et al. 1948; Ulloa Santana et al. 2011) (Fig. 15).

Davis et al. (1957) and Roy (2001) displayed the gravity map over a chromite ore in the Camagüey Area, Cuba (Fig. 16). From this figure, the marked black line with 180 m length was taken to represent the residual gravity profile (Fig. 17). This profile was digitized at an equal interval of 18 m. For the purpose of guessing z, s_n and K via the analytical signal of the gravity data, the suggested algorithm was utilized (Fig. 18) as shown in Table 5.

The optimum inverse parameters at minimum SD (SD = 4.18 m and SD = 1.38 m in cases of z and K, respectively) are given at $s_n = 1$, z = 49.49 m and K = 16.4 mGal × m^2. The best-fit-model is shown in Fig. 14 (open circle). This recommends that the suppressed structure shape is a cylinder model with 49.5 m depth. The estimated parameters (shape and depth) of the ore body were matched with those attained by different published interpreted methods (Table 6). Table 6 explains that the application of the suggested method gives an optimal result ($\lambda = 0.083$ mGal) for the buried mineral target, especially the depth, which opens the field for more investigations in the future using different methods.

Manganese ore body

Sarkar et al. (1967) demonstrated in detail the geology of the Nagpur area,

India is covered by soil with very scanty rock exposures. Rocks have suffered three phases of major folding deformation as revealed by surface and sub-surface data. These rock
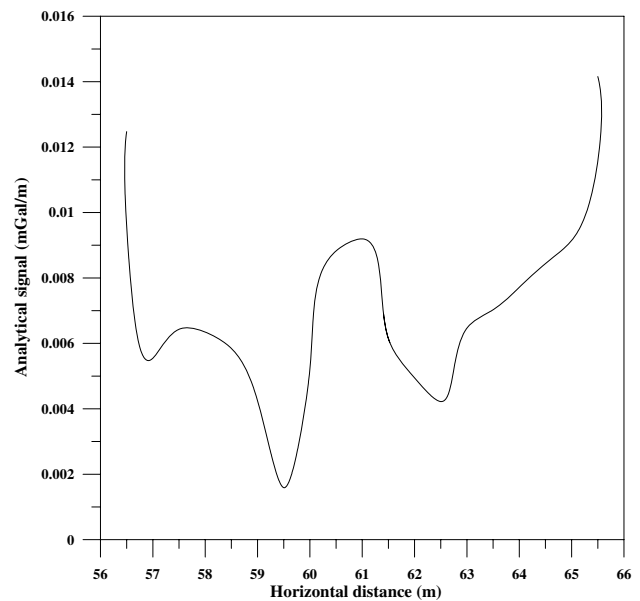
Fig. 14 Analytical signal of the anomaly in Fig. 13

Fig. 15 Geologic map of the Camagüey area, Cuba (after Ulloa Santana et al. 2011)
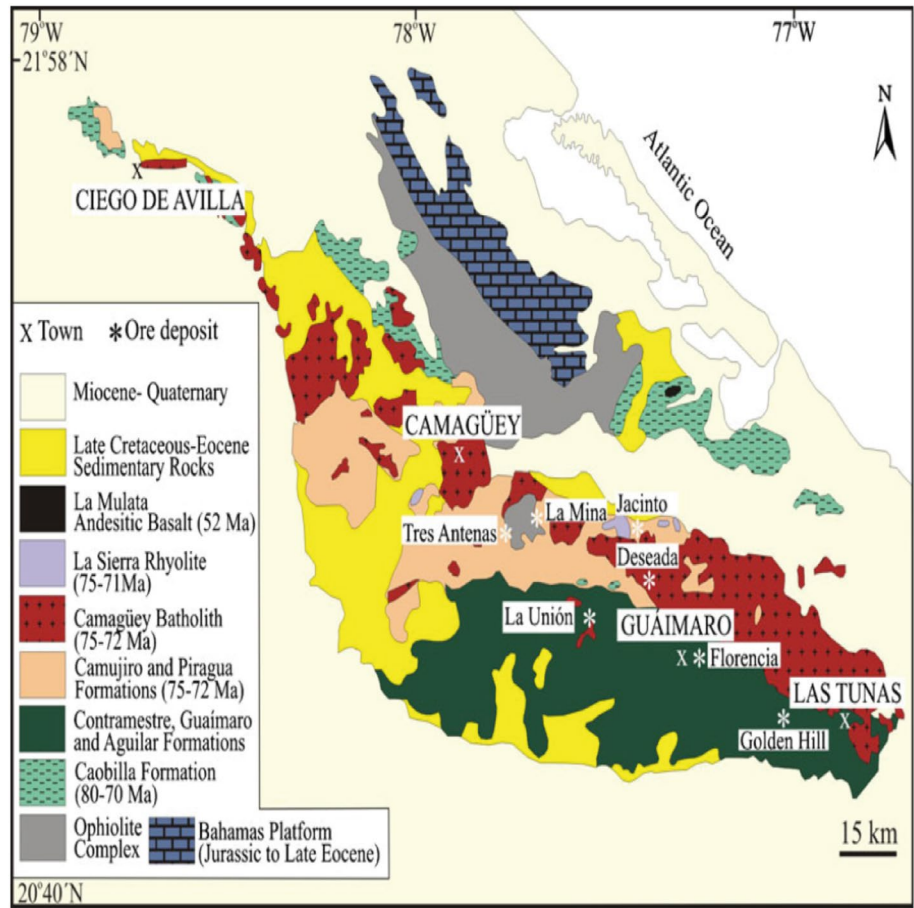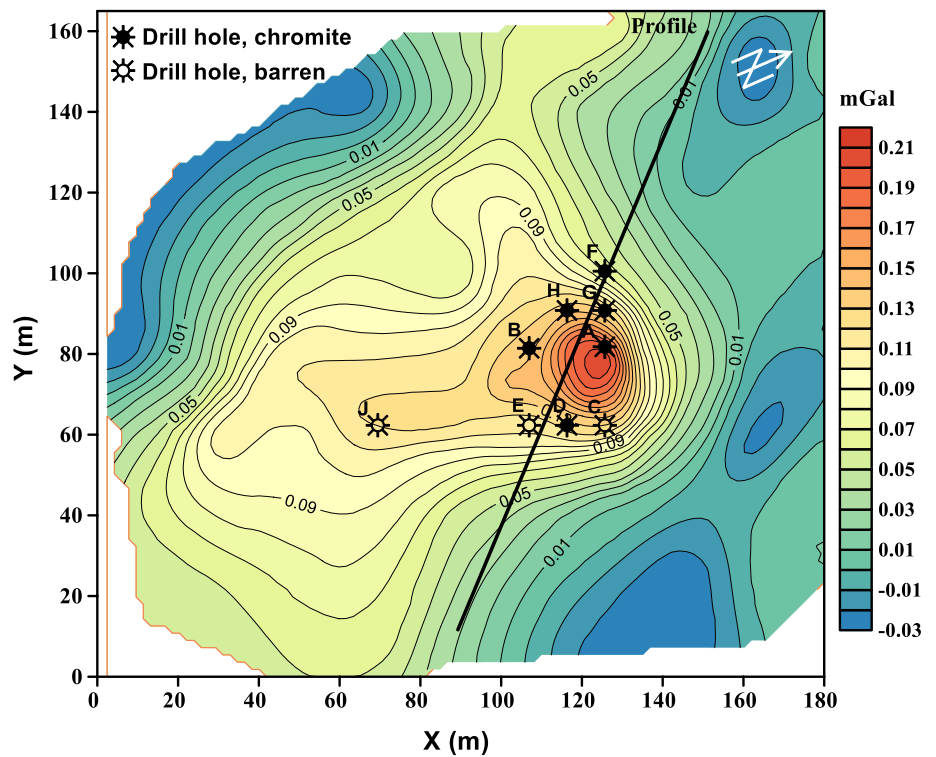

Fig. 16 Gravity anomaly map over a chromite deposit in the Camagüey area, Cuba (after Davis et al. 1957), the black line (Profile) represents the profile used in this study
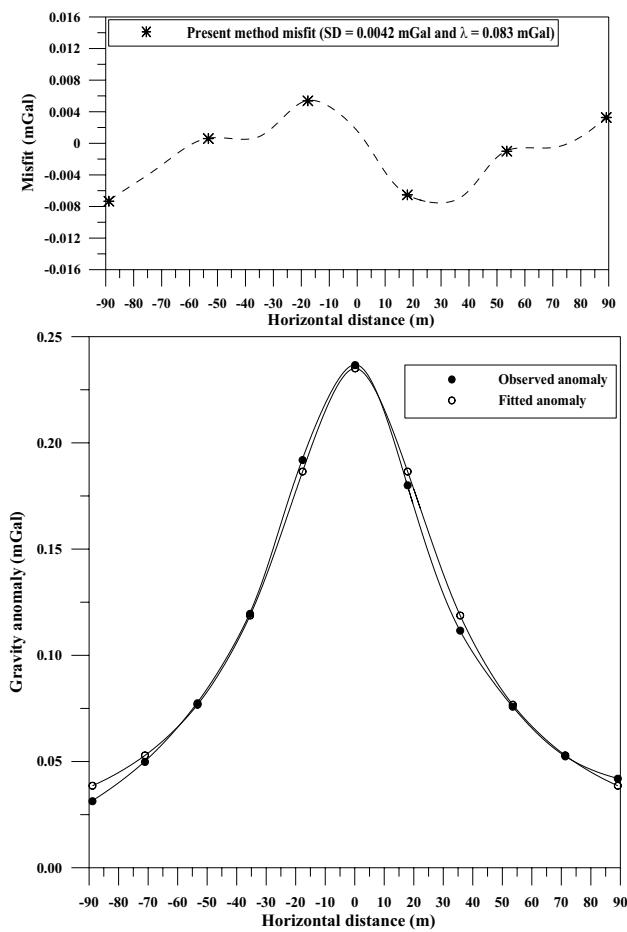
Fig. 17 Upper panel: The misfit between the observed and calculated data. Lower panel: A residual gravity anomaly (black circles) over a chromite body in Camagüey district, Cuba, and the predicted response (open circles) calculated from the present method

units denote series of anti-formal and syn-formal structures with steep plunge sub-parallel to strike Manganese oxide orebodies and manganese silicate rocks characterizing the metasedimentary sequence of the Precambrian rocks in the Nagpur area.

Reddi et al. (1995) show the gravity map over a manganese deposit near Nagpur, India (Fig. 19). A residual gravity profile was taken for this study area (Fig. 20). To show the residual gravity profile of the study area, a 333 m profile was digitized with an interim of 27 m (Fig. 20) and subjected to the inversion utilizing the present method. The new approach was utilized to the gravity data to appraise z, s_n and A utilizing the analytical signal of the gravity data (Fig. 21). The results are illustrated in Table 7.

The minimum SD was found at $s_n = 1$, $z = 59.77$ m and $K = 23.22$ mGal $\times$ m. The synthetic anomaly of the optimum parameters is shown in Fig. 20 (open circle). The results suggest that the shape of the buried target is a horizontal cylinder model buried at a depth of 59.77 m. The shape and the depth assessed by the present approach are in good agreement with those attained from Roy (2001), Essa (2012 and 2014), and Ekinci et al. (2016) (Table 8). Table 8 explains that our method gives the least root mean squared error ($\lambda = 0.048$ mGal). In other words, the estimated result, especially the depth of the target structure by the application of the proposed method is giving a powerful insight into the geologic subsurface.

The findings also emphasize that the real structures may not have the classic shapes (e.g. spheres or cylinders) or structures in nature. Therefore, the modeling and inversion of the real data mentioned-above with regular geometric-structures does not revenue the real subsurface targets. Insignificant deviation of the real-structure from the modeled

Table 5 Numerical results of the present method applied to a chromite body in Camagüey district, Cuba

M (m)	$s_n = 0.5$		$s_n = 1.0$		$s_n = 1.5$	
	Estimated depth (m)	Estimated amplitude coeff (mGal $\times$ m)	Estimated depth (m)	Estimated amplitude coeff (mGal $\times$ m^2)	Estimated depth (m)	Estimated amplitude coeff (mGal $\times$ m^3)
36.00	490.03	26.04	44.60	14.79	86.48	338.39
54.00	547.95	29.11	47.90	15.88	98.36	497.81
72.00	598.32	3.79	51.18	16.97	110.65	708.83
90.00	642.21	34.12	54.29	18.00	122.88	970.81
Average	569.62	30.27	49.49	16.41	104.59	628.96
SD	65.55	3.48	**4.18**	**1.38**	15.69	273.78

Bold indicates the true average values at the minimum SD

Table 6 A Comparative model parameters results for the chromite body in Camagüey district, Cuba

| Parameters	Mehanee method (2014)	Biswas method (2015)	The present method
A	$18.00 \text{ mGal} \times \text{m}^2$	$16.80 \text{ mGal} \times \text{m}$	$16.41 \text{ mGal} \times \text{m}$
z (m)	47.00	42.30	49.49
s_n (dimensionless)	1.5 (estimated)	1.0 (assumed)	1.0 (estimated)
λ (mGal)	0.121	0.103	**0.083**

*λ is the root mean squared error between the observed and calculated gravity anomalies

Bold indicates the true average values at the minimum SD

Table 7 Numerical results of the present method applied to a manganese deposit near Nagpur, India

M (m)	$s_n = 0.5$		$s_n = 1.0$		$s_n = 1.5$	
	Estimated depth (m)	Estimated amplitude coeff (mGal × m)	Estimated depth (m)	Estimated amplitude coeff (mGal × m²)	Estimated depth (m)	Estimated amplitude coeff (mGal × m³)
54.00	88.69	200.30	63.25	24.84	112.78	342.40
81.00	94.91	202.45	64.28	25.33	123.38	448.35
108.00	92.28	215.17	57.39	22.11	124.10	456.17
135.00	98.51	222.26	58.26	22.51	135.20	589.95
162.00	100.54	231.89	55.65	21.31	141.51	676.36
Average	94.99	214.41	59.77	23.22	127.40	502.65
SD	4.75	13.32	**3.79**	**1.77**	11.19	130.94

Bold indicates the true average values at the minimum SD

Table 8 A Comparative model parameters results for the manganese deposit near Nagpur, India

Parameters	Roy method (2001)	Essa method (2012)	Essa method (2014)	Ekinci et al. method (2016)	The present method
A (mGal × m)	–	7.91	17.81	14.2	23.22
z (m)	59.80	59.18	56.78	51.55	59.77
s_n (dimensionless)	–	1.15 (estimated)	1.15 (estimated)	1.00 (estimated)	1.00 (estimated)
λ (mGal)	–	0.127	0.102	0.128	**0.048**

*λ is the root mean squared error between the observed and calculated gravity anomalies

Bold indicates the true average values at the minimum SD

Fig. 18 Analytical signal of the anomaly in Fig. 17
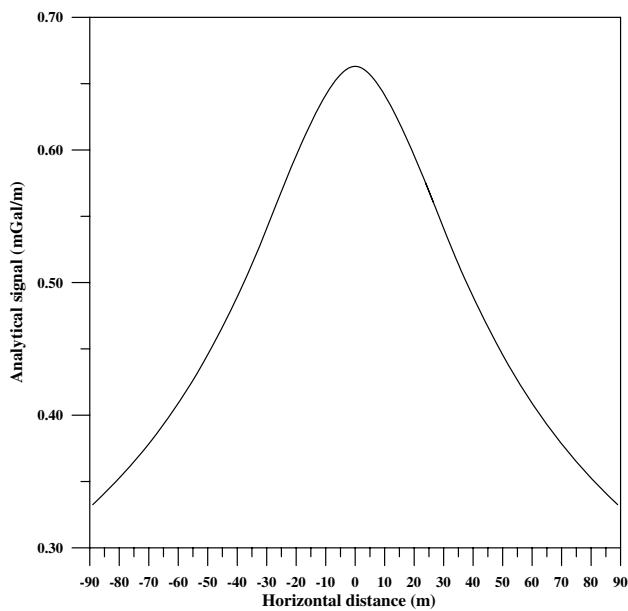
structure (e.g. spheres, cylinders) can be presumed to be a superposition of various types of noises on the responses represented by simple and standard geometric-structures. Hence we can catch a respectable estimation for the place and the depth of the subsurface structure of a mineralized target. Finally, it is important to mention that the suggested method can elucidate the gravity data for two mineralized structures from Cuba and India that have given a respectable result.

Fig. 19 Gravity anomaly map over a manganese deposit near Nagpur, India (after Reddi et al. 1995), the black line (Profile) represents the profile used in this study
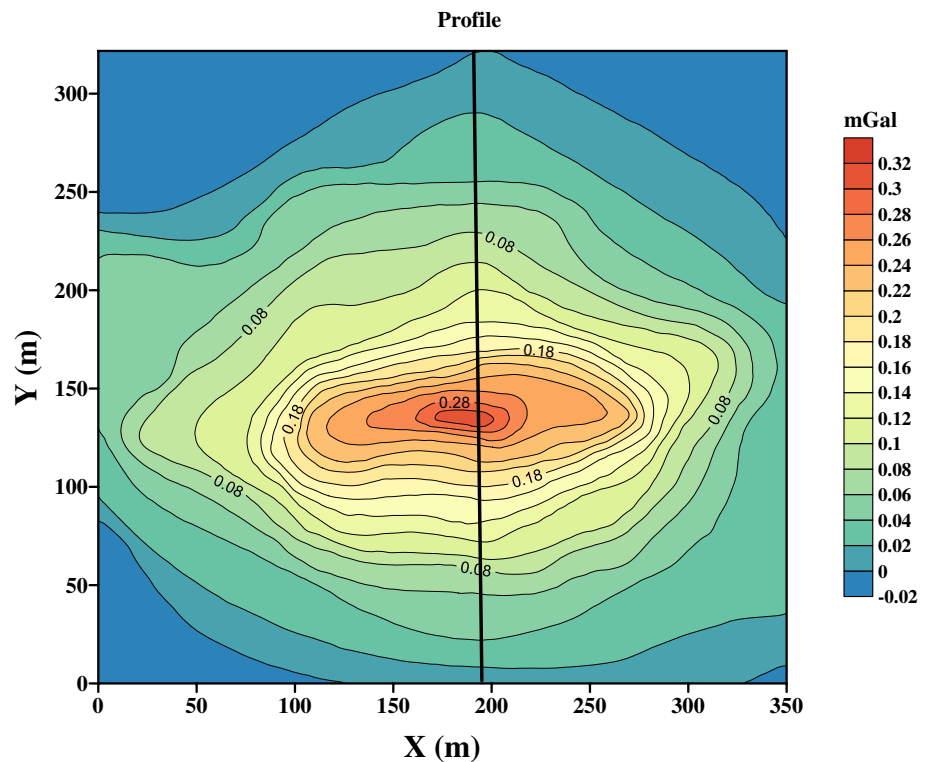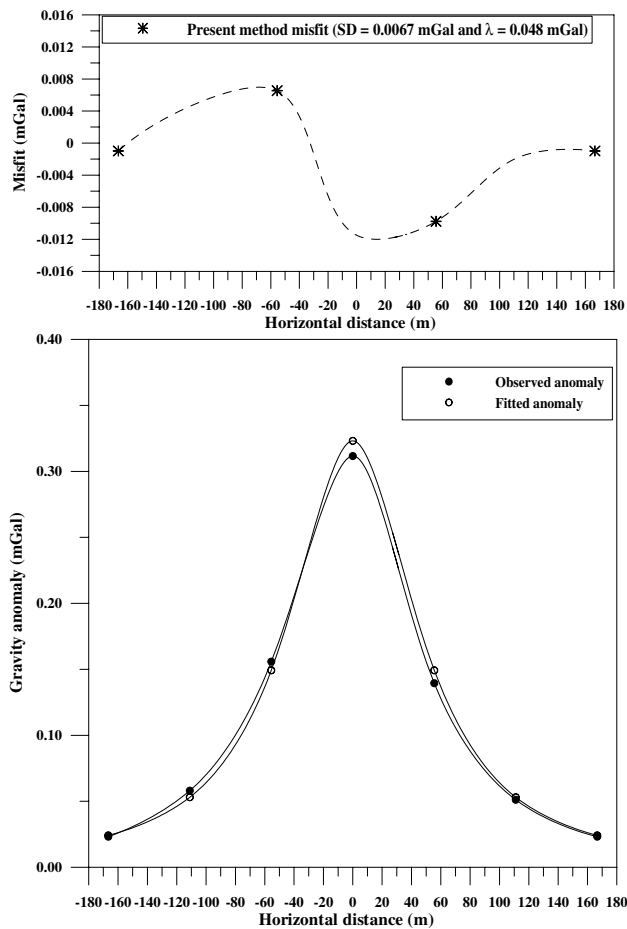
Fig. 20 Upper panel: The misfit between the observed and calculated data. Lower panel: The measured gravity anomaly (black circles) over a manganese deposit near Nagpur, India and the fitted response (open circles) computed from the present method
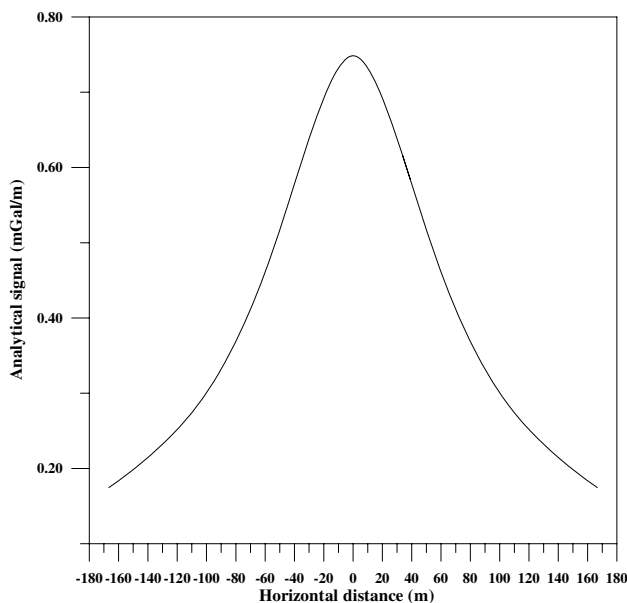
Fig. 21 Analytical signal of the anomaly in Fig. 20

Conclusion

The aim of our study was to assess the target buried structure parameters depth, shape, and the amplitude coefficient from the residual gravity data. The method used in this study relies on evaluating the analytical signal of the original gravity data and it utilizes the combination of all available points on the analytic signal profile to appraise the buried target parameters. The findings of this study revealed that our method was less affected by noise than other methods. In this regard, synthetic data, noisy data, and raw data, crypt example from Slovakia, and two mineralized examples from Cuba and India, were used to display and demonstrate the stability and efficiency of the suggested method. Thus, the inverted parameters (z, s_n) should be engaged by the available geological information and other provided geophysical outcomes to help in rectifying any encountered uncommon solution in geophysical exploration. While this proposed method was utilized for the simplified models, it provides an appropriate explanation for the new geological insight into the subsurface. However, this study is subject to a limitation which is the suggested method falls in the region of more complex and complicated structures which may cause more ambiguity in the results. Future line of research may overcome the above-declared facts by extending the use of this method in deciphering several problems.

References

Abdelrahman EM, Essa KS (2013) A new approach to semi-infinite thin slab depth determination from second moving average residual gravity anomalies. Explor Geophys 44:185–191

Abdelrahman EM, Essa KS (2015) Three least-squares minimization approaches to interpret gravity data due to dipping faults. Pure Appl Geophys 172:427–438

Abdelrahman EM, El-Araby HM, El-Araby TM, Essa KS (2002) A numerical approach to depth determination from magnetic data. Kuwait J Sci Eng 29:121–134

Abdelrahman EM, El-Araby TM, Essa KS (2003) Shape and depth solutions from third moving average residual gravity anomalies using the window curves method: Kuwait. J Sci Eng 30:95–108

Abdelrahman EM, Abo-Ezz ER, Essa KS, El-Araby TM, Soliman KS (2006) A least-squares variance analysis method for shape and depth estimation from gravity data. J Geophys Eng 3:143–153

Abedi M, Afshar A, Ardestani VE, Norouzi GH, Lucas C (2009) Application of various methods for 2D inverse modeling of residual gravity anomalies. Acta Geophys 58:317–336

Ansari AH, Alamdar K (2010) An improved method for geological boundary detection of potential field anomalies. Journal of Mining and Environment 2:37–44

Asfahani J, Tlas M (2008) An automatic method of direct interpretation of residual gravity anomaly profiles due to spheres and cylinders. Pure Appl Geophys 165:981–994

Asfahani J, Tlas M (2015) Estimation of gravity parameters related to simple geometrical structures by developing an approach based on deconvolution and linear optimization techniques. Pure Appl Geophys 172(10):2891–2899

Biswas A (2015) Interpretation of residual gravity anomaly caused by a simple shaped body using very fast simulated annealing global optimization. Geosci Front 6:875–893

Biswas A, Parija MP, Kumar S (2017) Global nonlinear optimization for the interpretation of source parameters from total gradient of gravity and magnetic anomalies caused by thin dyke. Ann Geophysics 60:G0218

Cella F, Fedi M, Florio G, Paoletti V, Rapolla A (2008) A review of the gravity and magnetic studies in the Tyrrhenian Basin and its volcanic districts. Ann Geophysics 51:3078

Davis WE, Jackson WH, Richter DH (1957) Gravity prospecting for chromite deposits in Camaguey Province. Cuba Geophysics 22:848–869

Ekinci YL, Balkaya C, Göktürkler G, Turan S (2016) Model parameter estimations from residual gravity anomalies due to simple-shaped sources using differential evolution algorithm. J Appl Geophys 129:133–147

Ekinci YL, Özyalın Ş, Sındırgı P, Balkaya Ç, Göktürkler G (2017) Amplitude inversion of the 2D analytic signal of magnetic anomalies through the differential evolution algorithm. J Geophys Eng 14:1492–1508

Eshaghzadeh A, Dehghanpour A, Sahebari SS (2019) Marquardt inverse modeling of the residual gravity anomalies due to simple geometric structures: a case study of chromite deposit. Contrib to Geophys Geodesy 49:153–180

Essa KS (2007a) A simple formula for shape and depth determination from residual gravity anomalies. Acta Geophys 55:182–190

Essa KS (2007b) Gravity data interpretation using s-curves method. J Geophys Eng 4:204–213

Essa KS (2011) A new algorithm for gravity or self-potential data interpretation. J Geophys Eng 8:434–446

Essa KS (2014) New fast least-squares algorithm for estimating the best-fitting parameters due to simple geometric-structures from gravity anomalies. J Adv Res 5:57–65

Essa KS, Munschy M (2019) Gravity data interpretation using the particle swarm optimization method with application to mineral exploration. J Earth Syst Sci 128:123

Essa, K.S. (2012). A fast least-squares method for inverse modeling of gravity anomaly profiles due simple geometric-shaped structures. Near Surface Geoscience 2012, 18th European Meeting of Environmental and Engineering Geophysics, Paris, France.

Essa, K.S., and Y. Géraud (2020). Parameters estimation from the gravity anomaly caused by the two-dimensional horizontal thin sheet applying the global particle swarm algorithm. J. Petrol. Sci. Eng., 193, 107421.

Essa, K.S., S.A. Mehanee and M. Elhussein (2021). Gravity data interpretation by a two-sided fault-like geologic structure using the global particle swarm technique. Phys. Earth Planet. Inter., 311, 106631.

Essa, K.S. (2013). Gravity interpretation of dipping faults using the variance analysis method. J. Geophys. Eng., 10, 015003.

Flint, D.E., J.F. De Albear and P.W. Guild (1948). Geology and chromite deposits of the Camagüey District Province, Cuba. United States Geological Survey Bulletin, 954–B, p.39–63.

Gupta OP (1983) A least-squares approach to depth determination from gravity data. Geophysics 48(3):357–360

Hinze WJ, von Frese RRB, Saad AH (2013) Gravity and magnetic exploration – principles, practices, and applications. Cambridge University Press

Kilty TK (1983) Werner deconvolution of profile potential field data. Geophysics 48:234–237

Mehanee SA (2014) Accurate and efficient regularized inversion approach for the interpretation of isolated gravity anomalies. Pure Appl Geophys 171:1897–1937

Mehanee, S.A. and K.S. Essa (2015). 2.5D regularized inversion for the interpretation of residual gravity data by a dipping thin sheet: numerical examples and case studies with an insight on sensitivity and non-uniqueness. Earth Planets and Space, 67, 130.

Nabighian MN (1972) The analytic signal of two-dimensional magnetic bodies with polygonal cross-section: Its properties and use for automated anomaly interpretation. Geophysics 37:507–517

Nettleton LL (1976) Gravity and Magnetics in Oil Prospecting. McGraw-Hill Book Co, New York

Odegard ME, Berg JW (1965) Gravity interpretation using the Fourier integral. Geophysics 30:424–438

Panisov J., R. Pasteka (2009). The use of microgravity technique in archaeology: A case study from the St. Nicolas Church in Pukanec, Slovakia, Contributions to Geophysics and Geodesy Vol. 39/3, 2009 (237–254).

Press WH, Flannery BP, Teukolsky SA, Vetterling WT (2007) Numerical Recipes. Cambridge University Press, New York, The Art of Scientific Computing

Reddi, A.B., B.R. Murthy and M. Kesavanani (1995). A compendium of four decades of geophysical activity in geological survey of India, GSI Spec. Publ., Geol. Surv. India 36, 46.

Roy L (2001) Short note: source geometry identification by simultaneous use of structural index and shape factor. Geophys Prospect 49:159–164

Sarkar SN, Gerling EK, Polkanov AA, Chukrov FV (1967) Pre-Cambrian Geochronology of Nagpur-Bhandara-Drug, India. Geol Mag 104:525–549

Srivastava S, Agarwal BNP (2010) Inversion of the amplitude of the two-dimensional analytic signal of the magnetic anomaly by the particle swarm optimization technique. Geophys J Int 182:652–662

Thompson DT (1982) EULDPH — A new technique for making computer-assisted depth estimates from magnetic data. Geophysics 47:31–37

Tlas M, Asfahani J (2019) Multiple-linear regression to best-estimate of gravity parameters related to simple geometrical shaped structures. Contrib to Geophys Geodesy 49:303–324

Ulloa Santana MM, Moura M, Olivo G, Botelho N, Bhn B (2011) The La Union Au Cu prospect, Camagüey District, Cuba: fluid inclusion and stable isotope evidence for ore-forming processes. Miner Deposita 46:91–104